Numerical Error in Electron Orbits with Large $\omega_{ce} \Delta t$

S. E. PARKER AND C. K. BIRDSALL

Electronics Research Laboratory, University of California, Berkeley, California 94720

We have found that running electrostatic particle codes at relatively large $\omega_{ce} \Delta t$ in some circumstances does not significantly affect the physical results. We first present results from a single particle mover finding the correct first order drifts for large $\omega_{ce} \Delta t$. We then characterize the numerical orbit of the Boris algorithm for rotation when $\omega_{ce} \Delta t \gg 1$. Next, an analysis of the guiding center motion is given showing why the first order drift is retained at large $\omega_{ce} \Delta t$. Lastly, we present a plasma simulation of a one dimensional cross field sheath, with large and small $\omega_{ce} \Delta t$, with very little difference in the results. © 1991 Academic Press, Inc.

1. INTRODUCTION

We have been using a bounded two-dimensional electrostatic particle code [1] to study cross field sheaths [2] and electrostatic effects produced by nonuniform magnetic fields [3]. We found that running with "unacceptably" large values of $\omega_{ce} \Delta t$ (~ 4) did not appear to cause any significant problems in these simulations. Hence, we address the issue of why plasma simulation with large $\omega_{ce} \Delta t$ under certain circumstances can produce physically acceptable results.

When numerically simulating a magnetized plasma with particle eletrons, the limiting time scale in some situations is the electron cyclotron period, with a constraint on $\omega_{ce} \Delta t$. However, under circumstances in which we are not interested in the short time scale physics, this constraint can make simulation of other effects at longer time scales very expensive. In explicit simulations, the requirement that $\omega_{pe} \Delta t$ be small for stability often determines the limit on Δt rather then ω_{ce}. However, in implicit particle simulations where the $\omega_{pe} \Delta t$ constraint has been relaxed, the requirement of small $\omega_{ce} \Delta t$ can be especially restrictive. Implicit simulations have been done with large $\omega_{ce} \Delta t$ by decentering the particle advance slightly which damps out the gyromotion [4]. Another method is to use the guiding center equations for electrons [5] to remove the $\omega_{ce} \Delta t$ timescale. It is also possible to use special values of $\omega_{ce} \Delta t$ (with $\omega_{ce} \Delta t \gg 1$) that satisfy Eq. (3) below and use the rotation method of Buneman [6, 7]. The Buneman method has been analyzed previously in Ref. [6] and does not produce the correct drift motion for large, arbitrary $\omega_{ce} \Delta t$.

We have chosen to explore the feasibility of running with large $\omega_{ce} \Delta t$ using the standard $\mathbf{v} \times \mathbf{B}$ rotation scheme of Boris [8, 9]. The reason for doing this, besides

91

simplicity, is that for modeling systems with a nonuniform magnetic field, $\omega_{ce} \Delta t$ can vary greatly (e.g., at a field null point) and Δt would need to be restricted by the largest value of ω_{ce}. In such a problem one cannot necessarily assume guiding center motion throughout the system because there may be regions of weak magnetization.

We begin by showing single particle orbits obtained with large $\omega_{ce} \Delta t$ and compare those to more exact orbits obtained with small $\omega_{ce} \Delta t$. Then, we discuss the orbit characteristics when $\omega_{ce} \Delta t$ is large. Next, an analysis of the the guiding center motion is given obtaining correct first order drifts. Finally, we show a collective model with many particles in which the results appear to be only slightly affected by using large $\omega_{ce} \Delta t$.

2. RESULTS FROM A SINGLE PARTICLE MOVER FOR $\omega_{ce} \Delta t \gg 1$

In order to study the errors introduced by using large $\omega_{ce} \Delta t$, we used the Boris mover in three dimensions on a single particle. The first four figures show single particle orbits with both large and small $\omega_{ce} \Delta t$. The converged orbit ($\omega_{ce} \Delta t$ small) is the "thick" center line and the large $\omega_{ce} \Delta t$ orbit oscillates alternately above and below the true orbit each step. The correct drift motion is retained but there is a numerically induced oscillation radius we will call r_{os}, and an oscillation frequency we will call ω_{os}, which is a numerical alteration of the true gyroradius and gyrofrequency. We will discuss this oscillation further in the following section. The charge to mass ratio was set equal to negative one for all the following runs ($q/m = -1$).

Figure 1 shows the $\mathbf{E} \times \mathbf{B}$ drift motion for two cases: $\omega_{ce} \Delta t = 0.5$ and 50. The following parameters are the same for both cases: $\mathbf{v}(t=0) = (0.1, 0.0, 0.4)$, $\mathbf{B} = (250, 0, 0)$, and $\mathbf{E} = (0, 0, 1)$. The $\mathbf{E} \times \mathbf{B}$ drift velocity is measured as $0.004\hat{y}$, as expected from $v_y = E_z/B_x$ and the total time $T = 100$. For the run with $\omega_{ce} \Delta t = 50$; $r_{os} \approx v_\perp \Delta t/2$, and $\omega_{prec} \approx 0.4$ as expected from the calculation in Section 3.

Figure 2 shows two runs with $\omega_{ce} \Delta t = 0.5$ and 16. In these runs the magnetic field is that caused by a line current along $\hat{z}$, centered at $(x, y) = (10, 10)$. B is given by: $\mathbf{B} = (800/r)\theta$. The initial position and velocity were: $\mathbf{x}(t=0) = (0, 10, 0)$, and $\mathbf{v}(t=0) = (0.16, 1, 0)$; and the total time was: $T = 200$. The particle has a parallel velocity component, v_θ, and follows the associated field line in the $x - y$ plane (circular motion). The curvature drift velocity is measure to be $1.25 \times 10^{-3}\hat{z}$ as predicted.

Figure 3 shows the $\mathbf{B} \times \nabla B$ drift motion due to $v_\perp$ for $\omega_{ce} \Delta t = 0.5$ and 50. The magnetic field is: $\mathbf{B} = (100 - 25y)\hat{x}$, and the initial velocity is: $\mathbf{v}(t=0) = (0, 0, 2)$, giving a drift velocity of: $\mathbf{v}_{\nabla B} = 0.005\hat{z}$.

Figure 4 shows the polarization drift motion with $\omega_{ce} \Delta t$ equal to 0.5 and 50. The fields are: $\mathbf{E} = -2t\hat{y}$ and $\mathbf{B} = 100\hat{x}$. The initial velocity is: $\mathbf{v}(t=0) = (0, 0, 0.1)$, giving a drift velocity of: $\mathbf{v}_p = 2 \times 10^{-4}\hat{y}$.
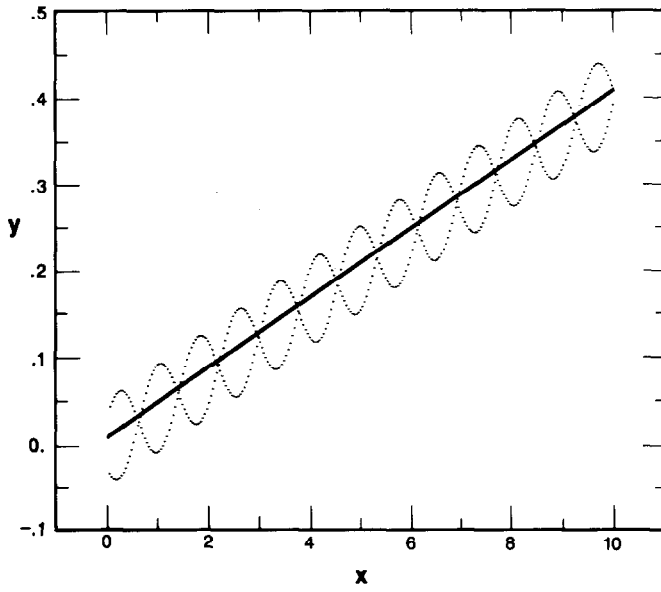
FIG. 1. $\mathbf{E} \times \mathbf{B}$ drift. Two cases: $\omega_{ce}\,\varDelta t = 0.5$ (thick line) and $\omega_{ce}\,\varDelta t = 50$.
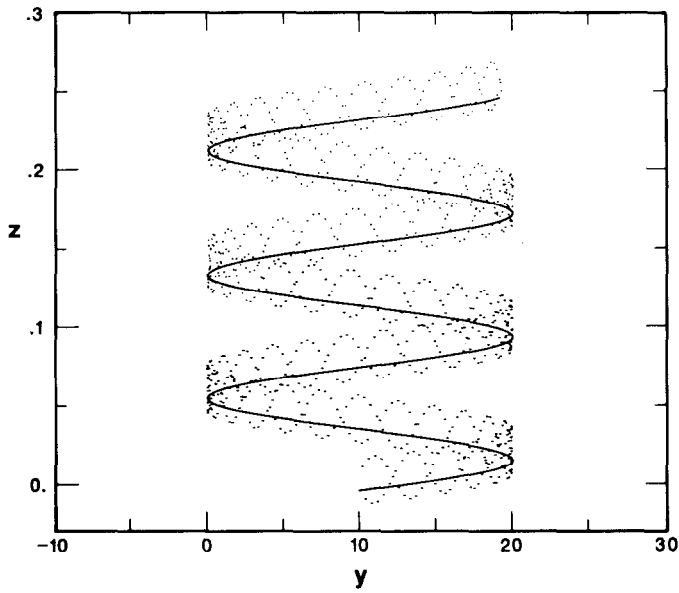
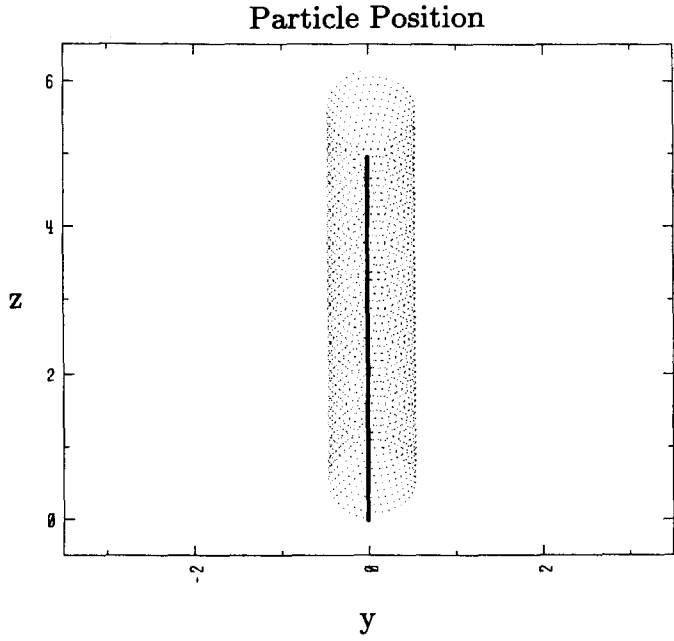FIG. 2. Curvature drift. Two cases: $\omega_{ce}\,\varDelta t = 0.5$ and 16.

Particle Position

FIG. 3. Gradient B drift. Two cases: $\omega_{ce} \Delta t = 0.5$ and 50.
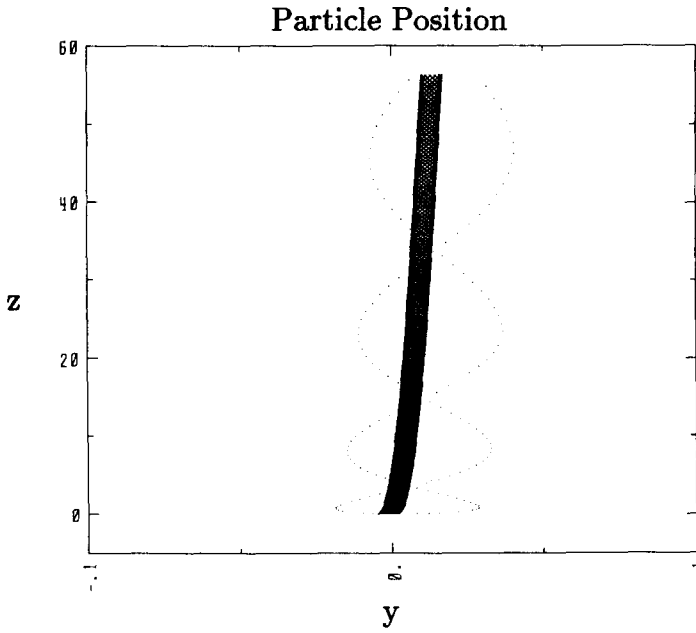
Particle Position

FIG. 4. Polarization drift. Two cases: $\omega_{ce} \Delta t = 0.5$ and 50.

We have also tested bounce motion in a simple mirror field producing the correct drift motion with large $\omega_{ce}\,\Delta t$ (see Ref. [10]). Note that in all these examples the averaged orbits (or drifts) are approximately equal. As long as r_{os} is small compared to the scale lengths of interest, then the drift plus the oscillatory motion may be acceptable in many particle plasma simulations.

3. Orbit Characteristics with $\omega_{ce}\,\Delta t \gg 1$

In this section we characterize the electron orbit when $\omega_{ce}\,\Delta t$ is large. The following analysis applies to single particle motion for any particle, but we focus on electrons since they have the most limiting time and space scales in conventional plasma simulations. We assume that the Lorentz equation is approximated with a finite difference equation similar to that of Buneman [11] having the form

$$\frac{1}{\Delta t}(\mathbf{v}^{n+1/2} - \mathbf{v}^{n-1/2}) = \frac{q}{m}\left\{\bar{\mathbf{E}}^n + \frac{1}{2}(\mathbf{v}^{n+1/2} + \mathbf{v}^{n-1/2}) \times \bar{\mathbf{B}}^n\right\}, \tag{1}$$

where $\bar{\mathbf{E}}^n$ is the difference operator approximating $\mathbf{E}(\mathbf{x}^n, t^n)$ to second order in time, and likewise for $\bar{\mathbf{B}}^n$. For example, the explicit leapfrog method would use: $\bar{\mathbf{E}}^n = \mathbf{E}(\mathbf{x}^n, t^n)$. An implicit example is the D1 scheme [11]: $\bar{\mathbf{E}}^n = \frac{1}{2}(\mathbf{E}(\mathbf{x}^{n+1}, t^{n+1}) + \bar{\mathbf{E}}^{n-1}))$. With the new velocity, the particle is then spatially advanced using:

$$\frac{1}{\Delta t}(\mathbf{x}^{n+1} - \mathbf{x}^n) = \mathbf{v}^{n+1/2} \tag{2}$$

The $\mathbf{v} \times \mathbf{B}$ rotation scheme of Boris gives the angle of rotation for one time step as [8]:

$$\omega_{os}\,\Delta t = \theta = 2\,\mathrm{arc\,tan}(\tfrac{1}{2}\omega_{ce}\,\Delta t). \tag{3}$$

As $\omega_{ce}\,\Delta t \to \infty$, $\theta \to \pi$. The orbit for $\omega_{ce}\,\Delta t \gg 1$ can be described as rapid bounce back and forth motion (so-called odd–even motion) with the perpendicular velocity and a slow precession about the guiding center axis. For large $\omega_{ce}\,\Delta t$, the angle of rotation is approximately

$$\theta \approx \pi - \frac{4}{\omega_{ce}\,\Delta t}. \tag{4}$$

The precession is the result of the rotation angle being a small amount δ less than π, $\delta = \pi - \theta$. The frequency of this precession is

$$\omega_{prec} = \frac{\delta}{\Delta t} \approx \frac{4}{\omega_{ce}\,\Delta t}. \tag{5}$$

The rotation frequency is slightly less than $\pi/\Delta t$ (much less than ω_{cc}). We call this the "oscillation" frequency:

$$\omega_{os} \approx \frac{1}{\Delta t}\left(\pi - \frac{4}{\omega_{ce}\,\Delta t}\right). \tag{6}$$

Note that ω_{prec} goes to zero, and ω_{os} goes to $\pi/\Delta t$, for large $\omega_{ce}\,\Delta t$.

The gyroradius is also altered, we call this numerical gyroradius the oscillation radius. The oscillation radius for all values of $\omega_{ce}\,\Delta t$ is given by (see Fig. 4-3b in Ref. [8]):

$$r_{os} = \frac{v_\perp\,\Delta t}{2\sin(\theta/2)} = r_{ge}\left[1 + \left(\frac{\omega_{ce}\,\Delta t}{2}\right)^2\right]^{1/2}. \tag{7}$$

For large $\omega_{ce}\,\Delta t$, Eq. (7) reduces to

$$r_{os} \approx \tfrac{1}{2} v_\perp\,\Delta t. \tag{8}$$

Since $r_{os} \sim O(v_\perp\,\Delta t)$, not $O(\omega_{ce}\,\Delta t)$, the oscillation radius can still be small in strongly magnetized systems where $\omega_{ce}\,\Delta t$ is large.

4. GUIDING CENTER MOTION WITH $\omega_{ce}\,\Delta t \gg 1$

We now analyze the guiding center motion to see what error is introduced when $\omega_{ce}\,\Delta t$ is made large. We start with the difference scheme Eq. (1) and eliminate $\mathbf{v}$ using $\mathbf{v}^{n-1/2} = (\mathbf{x}^n - \mathbf{x}^{n-1})/\Delta t$ and, $\mathbf{v}^{n+1/2} = (\mathbf{x}^{n+1} - \mathbf{x}^n)/\Delta t$:

$$\frac{1}{\Delta t^2}(\mathbf{x}^{n+1} - 2\mathbf{x}^n + \mathbf{x}^{n-1}) = \frac{q}{m}\left\{\bar{\mathbf{E}}^n + \frac{1}{2\Delta t})\mathbf{x}^{n+1} - \mathbf{x}^{n-1}) \times \bar{\mathbf{B}}^n\right\}. \tag{9}$$

Let the magnetic field $\mathbf{B}$ be in the $x - y$ plane and define the following coordinates: $\hat{\mathbf{e}}_1 = \mathbf{B}/B$, $\hat{\mathbf{e}}_2 = \hat{\mathbf{z}}$, and $\hat{\mathbf{e}}_3 = \hat{\mathbf{e}}_1 \times \hat{\mathbf{e}}_2$. Let $\mathbf{x}^n = \mathbf{x}_0^n + \mathbf{x}_1^n$, where $\mathbf{x}_1^n = r_{os}^n(\sin\phi^n\hat{\mathbf{e}}_2 + \cos\phi^n\hat{\mathbf{e}}_3)$, and $\phi^n = \phi_0 + \Delta t\sum_{m=1}^n \omega_{os}^m$. $\mathbf{x}_0$ is the slowly varying guiding center motion, and $\mathbf{x}_1$ is the fast gyration. Assume that ω_{os} and r_{os} do not vary much between time steps so we can use the approximations: $\omega_{os}^n \approx \omega_{os}^{n+1}$ and $r_{os}^n \approx r_{os}^{n+1}$. Taking a Taylor series expansion of Eq. (9) about $\mathbf{x}_0$, and then equating the slowly varying terms gives the guiding center equation:

$$\frac{1}{\Delta t^2}(\mathbf{x}_0^{n+1} - 2\mathbf{x}_0^n + \mathbf{x}_0^{n-1}) = \frac{q}{m}\left\{\bar{\mathbf{E}}^n(\mathbf{x}_0^n) + \frac{1}{2\Delta t}(\mathbf{x}_0^{n+1} - \mathbf{x}_0^{n-1}) \times \bar{\mathbf{B}}^n(\mathbf{x}_0^n)\right\}$$

$$-\frac{\mu_{os}}{m}\nabla B(\mathbf{x}_0^n) + O\left(\frac{q}{m}r_{os}^2\right), \tag{10}$$

where $\mu_{os} = (qr_{os}^2/2\Delta t)\sin(\omega_{os}\,\Delta t)$. A more complete derivation of Eq. (10) is given in the Appendix. Using Eqs. (3) and (7), we find $\mu_{os} = \tfrac{1}{2}(v_\perp^2/B) = \mu$. Now,

substituting $x_0(t^n)$ for the approximate solution x_0^n and expanding about $x_0(t^n)$ we obtain the differential equation that the finite difference Eq. (10) approximates

$$\frac{d^2 x_0(t^n)}{dt^2} = \frac{q}{m} \left\{ E(x_0(t^n),\, t^n) + \frac{dx_0(t^n)}{dt} \times B(x_0(t^n),\, t^n) \right\} - \frac{\mu}{m} \nabla B(x_0(t^n),\, t^n)$$

$$+ O\left(\frac{q}{m} r_{os}^2\right) + O(\Delta t)^2. \tag{11}$$

The additional terms represented by $O(q/m\, r_{os}^2)$ are the higher order terms that where neglected in deriving Eq. (10). The terms represented by $O(\Delta t^2)$ are from the finite difference approximations for dx_0/dt and $d^2 x_0/dt^2$ that appear in Eq. (10).

The guiding center equation of motion given by Northrup [12] from which the first-order drifts are derived is

$$\frac{d^2 x_0}{dt^2} = \frac{q}{m} \left\{ E(x_0,\, t) + \frac{dx_0}{dt} \times B(x_0,\, t) \right\} - \frac{\mu}{m} \nabla B(x_0,\, t) + O\left(\frac{q}{m} r_g^2\right). \tag{12}$$

These are the same equations except for the higher order error terms. Assuming r_{os} is small compared to the field scale lengths, we expect the same first-order drift motion.

5. RESULTS FROM A ELECTROSTATIC PARTICLE CODE

In this section we present results from a collective simulation to show what happens at large $\omega_{ce}\,\Delta t$. We choose as a test problem a bounded plasma slab with a cross-field sheath (see Fig. 5). The model is one-dimensional spatially with two velocity components (x, v_x, v_y). There is a perpendicular constant magnetic field $(B = B_0 \hat{z})$. The boundary is a conducting wall parallel to the magnetic field. At the right boundary, all particles are absorbed that come in contact to it, and the electrostatic potential is allowed to float. At the left is an inversion symmetry plane
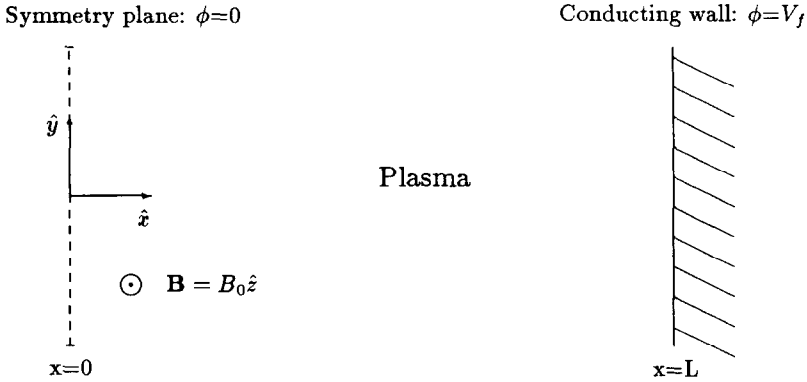

FIG. 5. Schematic of the test problem.

where particles are reflected and the plasma potential is set to zero. The code used
was PDW1 [13]. Table I gives the parameters used for the two test runs. We use
the MKSA units system but with ε_0 set equal to one. Alternatively, the units can
be described as dimensionless with length and time normalized by λ_{De} and ω_{pe}^{-1}. We
chose the parameters such that ω_{pe} was small compared to ω_{ce} to avoid errors due
to large $\omega_{pe} \Delta t$. Δt was varied to see what errors were introduced.

For this problem, the potential drop in the sheath is dependent on the disparity
between the ion and electron gyroradii. As long as r_{os} for the electrons is much less
than r_{gi} the results are not greatly affected. Figures 6 and 7 show results for two
runs, one with $\omega_{ce} \Delta t = 0.4$ and the other with $\omega_{ce} \Delta t = 8$. Figure 6 is a snapshot of
the spatial variation of the electrostatic potential at: $t = 1000$. Figure 7 is a plot of
the time evolution of the total potential drop, V_f. The potential drop is affected
slightly (-2%) for the large $\omega_{ce} \Delta t$ case due to increase in r_{os} causing more elec-
trons to hit the wall. The numerical value of r_{os} using Eq. (7) is $1.02r_{ge}$ for the
$\omega_{ce} \Delta t = 0.4$ case, and $4.12r_{ge}$ for the $\omega_{ce} \Delta t = 8$ case. There is no significant total
energy gain, hence we suspect there is no collective instability. The change in the
electron thermal energy and the total energy was very small for both runs (less than
0.1% for the time period of the run $1000\omega_{pe}$).

The time dependent behavior, Fig. 7, shows an initial transient where particles
within $\sim r_g$ of the wall are absorbed. This produces a net positive wall charge since
$r_{gi} > r_{ge}$. There is also a regular oscillation seen later in time measured at $\omega = 0.035$.
This measured quantity compares closely to the lower hybrid resonance [14]:

$$\omega^2 = \omega_{LH}^2 = \frac{\omega_{pi}^2 + \omega_{ci}^2}{(1 + \omega_{pe}^2/\omega_{ce}^2)}. \tag{13}$$

With the parameters in Table I: $\omega_{pe}^2/\omega_{ce}^2 = 6.25 \times 10^{-4} \ll 1$. For this range of
$\omega_{pe}^2/\omega_{ce}^2$ the lower hybrid resonance is approximately

$$\omega^2 = \omega_{pi}^2 + \omega_{ci}^2. \tag{14}$$

Equation (14) can be also be interpreted as an ion Bernstein mode [15] with
$k_\perp = 0$, obtained by assuming the electrons are fixed in the direction perpendicular
to **B** due to the strong magnetization.

TABLE I

Parameters for the Magnetized Sheath Test Run

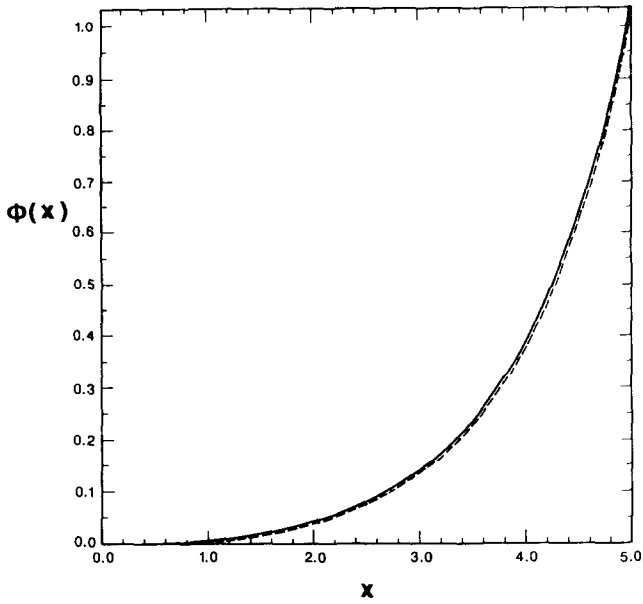| Parameters	$\Delta x = 0.1$	$\Delta t = 0.01, 0.2$	$L = 5.0$	$B = 40.0$
Electrons	$q/m = -1.0$	$q = -1 \times 10^{-3}$	$v_T = 1.0$	$N \approx 5000$
	$\omega_p = 1$	$\lambda_D = 1$	$\omega_c = 40.0$	$r_g = 0.025$
Ions	$q/m = 6.25 \times 10^{-4}$	$q = 1 \times 10^{-3}$	$v_T = 0.025$	$N \approx 5000$
	$\omega_p = 0.025$	$\lambda_D = 1$	$\omega_c = 0.025$	$r_g = 1$

FIG. 6. Electrostatic potential vs x, at $t = 1000$, for two cases: $\omega_{ce} \Delta t = 0.4$ (upper solid line) and $\omega_{ce} \Delta t = 8$ (lower dashed line).
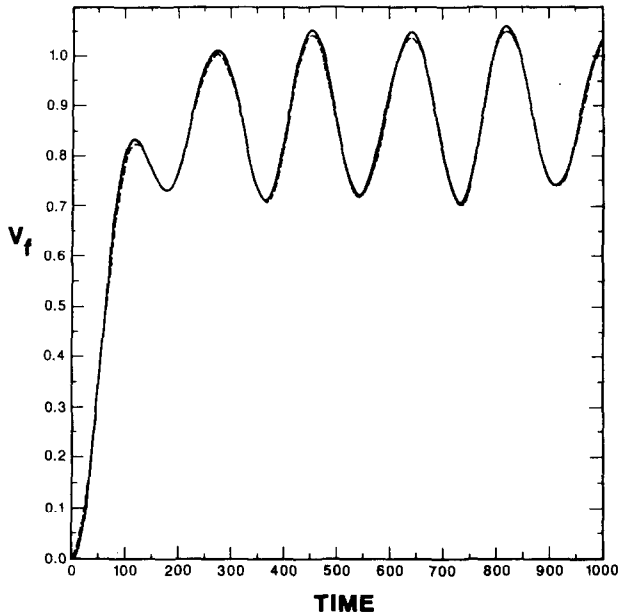

FIG. 7. Wall potential: V_f vs time for two cases: $\omega_{ce} \Delta t = 0.4$ (upper solid line) and $\omega_{ce} \Delta t = 8$ (lower dashed line).

In the results presented $\omega_{LH}\,\varDelta t \ll 1$ which allowed proper resolution of the lower hybrid oscillations. Because r_{os} is so small, the fluctuations associated with the electron cyclotron oscillations are much smaller than that of the lower hybrid (or ion Bernstein) oscillations. When $\omega_{ce}\,\varDelta t$ is large we are restricted to modeling physics with $r_{os}/\lambda_\perp \ll 1$, where $\lambda_\perp$ is the scale length of the electric field perpendicular to $\mathbf{B}$. However, for large mass ratio the ion gyro-orbit is fully resolved and therefore there is no restriction on $r_{gi}/\lambda_\perp$. The good results using large $\omega_{ce}\,\varDelta t$ depend on $r_{os} \ll r_{gi}$. Increasing the mass ratio improves the results. For example, reducing the mass ratio from 1600 to 100, and keeping $T_i = T_e$, produces an error of about -15% in the wall potential. The larger error for the case with smaller mass ratio is the result of reducing the ratio of r_{gi} to r_{os} (in this case by a factor of 4, $r_{gi} = 0.25$).

6. DISCUSSION

We conclude that even with $\omega_{ce}\,\varDelta t \gg 1$ the Boris algorithm for $\mathbf{v} \times \mathbf{B}$ rotation still produces very nearly the correct guiding center motion for a single particle. The error introduced is to increase the oscillation radius ($r_{ge} \to r_{os}$) and to decrease the oscillation frequency ($\omega_{ce} \to \omega_{os}$). The single particle motion can be described as a rapid odd–even bounce motion, bouncing $\frac{1}{2}v_\perp\,\varDelta t$ every time step and having a slow precession (ω_{prec}) about the guiding center.

This paper did not take into account the potential for collective instability. This has been previously addressed (see Ref. [8, pp. 201–202]). An electrostatic particle simulation of a one-dimensional cross-field sheath was presented. This particular problem showed that only slight errors resulted for large values of $\omega_{ce}\,\varDelta t$. There was no significant energy gain, thus no indication of collective numerical instability.

APPENDIX

Here we derive Eq. (10) more explicitly. This calculation is very similar to the derivation of Eq. (12) given in Ref. [12, p. 5]. The difference being that Eq. (9) is discrete and we cannot gyroaverage over the phase. Instead, we separate the motion into a fast oscillating part $\mathbf{x}_1$ and a slowly varying part $\mathbf{x}_0$, then we equate the slowly varying terms. Except for this difference, the derivations of Eq. (10) and Eq. (12) are analogous. Using Eq. (9) with $\mathbf{x}^n = \mathbf{x}_0^n + \mathbf{x}_1^n$ and expanding about $\mathbf{x}_0^n$ we arrive at

$$
\frac{1}{\varDelta t^2}(\mathbf{x}_0^{n+1} - 2\mathbf{x}_0^n + \mathbf{x}_0^{n-1} + \mathbf{x}_1^{n+1} - 2\mathbf{x}_1^n + \mathbf{x}_1^{n-1})
$$

$$
= \frac{q}{m}\left\{\bar{\mathbf{E}}^n(\mathbf{x}_0^n) + \frac{1}{2\varDelta t}(\mathbf{x}_0^{n+1} - \mathbf{x}_0^{n-1}) \times \bar{\mathbf{B}}^n(\mathbf{x}_0^n)\right\}
$$

$$
+ \frac{q}{m}\left\{(\mathbf{x}_1^n \cdot \nabla)\,\bar{\mathbf{E}}^n(\mathbf{x}_0^n) + \frac{1}{2\varDelta t}(\mathbf{x}_1^{n+1} - \mathbf{x}_1^{n-1}) \times \bar{\mathbf{B}}^n(\mathbf{x}_0^n)\right\}
$$

$$
+ \frac{q}{m}\frac{1}{2\varDelta t}(\mathbf{x}_1^{n+1} - \mathbf{x}_1^{n-1}) \times (\mathbf{x}_1^n \cdot \nabla)\,\bar{\mathbf{B}}(\mathbf{x}_0^n) + O\left(\frac{q}{m}r_{os}^2\right). \qquad (15)
$$

The third term on the right-hand side (we will call it RHS_3) is not higher order and has a slowly varying part as will be shown below. Subsituting $\mathbf{x}_1^n = r_{os}^n(\sin \phi^n \hat{\mathbf{e}}_2 + \cos \phi^n \hat{\mathbf{e}}_3)$ into RHS_3 and, assuming r_{os} and ω_{os} are slowly varying functions of time so that $r_{os}^{n-1} \approx r_{os}^n \approx r_{os}^{n+1}$ and $\omega_{os}^{n-1} \approx \omega_{os}^n \approx \omega_{os}^{n+1}$, we obtain

$$RHS_3 \equiv \frac{q}{m} \frac{1}{2\Delta t} (\mathbf{x}_1^{n+1} - \mathbf{x}_1^{n-1}) \times (\mathbf{x}_1^n \cdot \nabla) \, \bar{B}(\mathbf{x}_0^n) \tag{16}$$

$$= \frac{q}{m} \frac{1}{2\Delta t} (r_{os}^n)^2 \left\{ [\sin(\phi^n + \Delta t \omega_{os}^n) - \sin(\phi^n - \Delta t \omega_{os}^n)] \hat{\mathbf{e}}_2 \right.$$

$$+ \left. [\cos(\phi^n + \Delta t \omega_{os}^n) - \cos(\phi^n - \Delta t \omega_{os}^n)] \hat{\mathbf{e}}_3 \right\}$$

$$\times [(\sin \phi^n \hat{\mathbf{e}}_2 + \cos \phi^n \hat{\mathbf{e}}_3) \cdot \nabla] \, \bar{\mathbf{B}}(\mathbf{x}_0^n). \tag{17}$$

This can be further simplified to

$$RHS_3 = \frac{q}{m} \frac{(r_{os}^n)^2}{2\Delta t} \sin(\omega_{os}^n \Delta t)[\hat{\mathbf{e}}_2 \times (\hat{\mathbf{e}}_3 \cdot \nabla) \, \bar{\mathbf{B}}(\mathbf{x}_0^n)$$

$$- \hat{\mathbf{e}}_3 \times (\hat{\mathbf{e}}_2 \cdot \nabla) \, \bar{\mathbf{B}}(\mathbf{x}_0^n)] + f(\phi^n), \tag{18}$$

where we have written $f(\phi^n)$ to represent terms that rapidly oscillate about zero. It is seen from this equation that there is a slowly varying part of RHS_3. In Ref. [12, p. 5] the following result is obtained using $\nabla \cdot \mathbf{B} = 0$:

$$\hat{\mathbf{e}}_2 \times (\hat{\mathbf{e}}_3 \cdot \nabla) \mathbf{B} - \hat{\mathbf{e}}_3 \times (\hat{\mathbf{e}}_2 \cdot \nabla) \mathbf{B} = -\nabla \bar{B}. \tag{19}$$

Substituting Eq. (19) into Eq. (18) and using the definition of μ_{os} we obtain

$$RHS_3 = -\mu_{os} \nabla \bar{B}(\mathbf{x}_0^n) + f(\phi^n). \tag{20}$$

Finally, we equate all the slowly varying terms in Eq. (15) and use Eq. (20) for RHS_3. The resulting equation is Eq. (10).

REFERENCES

1. K. THIELHABER, "ES2 User's Manual-Version 1," ERL Report UCB/ERL M87/23, Electronics Research Laboratory, University of California, Berkeley, 1987 (unpublished).
2. K. THIELHABER AND C. K. BIRDSALL, *Phys. Rev. Lett.* **62**, 772 (1988).

3. S. E. PARKER, "Electrostatic Confinement due to Nonuniform Magnetic Fields with Application to FRC Confinement," ERL Report UCB/ERL M87/62, Electronics Research Laboratory, University of California, Berkeley, 1987 (unpublished).

4. D. C. BARNES, T. KAMIMURA, J. N. LEBOEUF, AND T. TAJIMA, *J. Comput. Phys.* **52**, 480 (1983).

5. W. W. LEE AND H. OKUDA, *J. Comput. Phys.* **26**, 139 (1978).

6. O. BUNEMAN, *J. Comput. Phys.* **1**, 111 (1967).

7. W. M. NEVINS, J. HARTE, AND Y. GELL, *Phys. Fluids* **22**, 2108 (1979).

8. C. K. BIRDSALL AND A. B. LANGDON, *Plasma Physics via Computer Simulation* (McGraw-Hill, New York, 1985).

9. J. P. BORIS, "Relativistic Plasma Simulation—Optimization of a Hybrid Code," Proceedings, Fourth Conference on Numerical Simulation of Plasmas, Washington DC, November 1970, pp. 3–67.

10. S. E. PARKER, "Nuermical Error in Electron Orbits with Large $\omega_{ce} \Delta t$," Proceedings, 12th Conference on Numerical Simulation of Plasmas, San Fransisco, CA, September 1987.

11. A. B. LANGDON AND D. C. BARNES, in *Multiple Time Scales*, in Computational Techniques, edited by J. U. Brackbill and B. I. Cohen (Academic Press, New York, 1985).

12. T. H. NORTHRUP, *The Adiabatic Motion of Charged Particles* (Wiley, New York, 1963).

13. W. M. LAWSON, *J. Comput. Phys.* **80**, 253 (1989).

14. G. SCHMIDT, *Physics of High Temperature Plasmas*, 2nd ed. (Academic Press, New York, 1979).

15. J. A. TATARONIS AND F. W. CRAWFORD, *J. Plasma Phys.* **4**, 231 (1970).